Metal-to-Multilayer-Graphene Contact—Part II: Analysis of Contact Resistance

Yasin Khatami, *Student Member, IEEE*, Hong Li, *Student Member, IEEE*, Chuan Xu, *Member, IEEE*, and Kaustav Banerjee, *Fellow, IEEE*

***Abstract*—The parasitic contact resistance between metal electrodes and multilayer graphene (MLG) is studied, and the different parameters influencing the contact resistance are investigated. A theoretical model that was developed in the companion paper is applied to typical metal–MLG structures to study the characteristics of the contact. The contributions of all of the three major components of resistance—the top and edge contacts (side and end contacts), the MLG sheet resistivity, and the metal sheet resistivity—to the total resistance are studied. The results show that the total resistance of the metal–MLG contact reduces substantially with the incorporation of edge contacts as the number of graphene layers increases. The current crowding effects are studied with and without consideration of the metal resistivity. Furthermore, the conditions where each of the three major resistance components becomes important are investigated. It is shown that the metal resistance can play an important role in determining the total resistance and current distribution in the contact. The developed model can be used in the characterization and in the design of efficient metal–MLG contact structures. It is shown that, due to the presence of edge contacts, the conventional methods of contact characterization cannot model the metal–MLG structure accurately.**

***Index Terms*—Contact resistance, edge contact, multilayer graphene (MLG), top contact, 1-D contact model.**

I. Introduction

GRAPHENE exhibits excellent electrical, mechanical, and thermal characteristics such as high mobility, high current density, high tensile strength, and high thermodynamic stability [1]–[6]. Multilayer graphene (MLG) which consists of several layers of single-layer graphene (SLG) has attracted researchers into the use of MLG in device and interconnect applications due to its high electrical and thermal conductivities [1]–[7] and also as transparent and flexible electrode materials in a number of applications. With the growing interest in MLG, the study and modeling of its parasitic components such as contact resistance become more important. The contact resistance can degrade the characteristics of various metal-MLG structures, and its effects must be accounted for.

Unlike metal contacts to conventional materials in electronic applications such as silicon, the metal-MLG contact structure includes both the edge and top contacts. The schematic illustration of the edge and top contacts is shown in the companion paper (part I) [8]. The edge contact is known to exhibit a resistivity much smaller than that of the top contact [9], [10]. The lower resistivity of the edge contact is attributed to the higher cohesive energy of the metal–carbon system in the edge contact compared to the top contact. The higher cohesive energy leads to a lower gap between the carbon and metal atoms and lower contact resistivity.

The existing models for characterization and analysis of the contact structures usually focus on structures with top contacts [11]–[14]. However, due to the existence of the edge contacts in the metal-MLG structure, a new model for the resistance of the system needs to be developed. In the companion paper [8], a 1-D model was developed for the metal-MLG structure with edge and top contacts by assuming a negligible metal resistivity. The 1-D model was compared to a 3-D model and was optimized to include the effects of the potential distribution along the width and thickness of MLG.

In this paper, the developed model in the companion paper [8] is applied to metal-MLG structures in Section III. Different resistivity values and geometries are considered with the assumption that the metal resistivity is negligible. This analysis provides insight into the role of edge contacts in metal-MLG structures and the main parameters influencing the total resistance of the structure. Then, in Section IV, the 1-D model is expanded to include the effect of metal resistance, and the full analysis of the metal-MLG structure is presented. In Section V, the developed model is extended for the quasi-ballistic transport. This type of analysis is invaluable for both the characterization and design of MLG-based structures that involve top and edge contacts.

II. Metal–MLG Contact Structure

The structure of the metal-MLG contact is adopted from the companion paper [8]. The dimensional parameters are defined in [8], where w and t are the width and thickness of the MLG sheet, respectively, L_C is the contact length, $w_{\rm sm}$ and $t_{\rm sm}$ are the width and thickness of the side metal, respectively, and L_m is the length of the extension of the metal. The sheet resistivity of SLG and the metal resistivity are represented by ρ_s and ρ_m, respectively, and their unit is ohm meter. The top contact

Manuscript received March 21, 2012; revised May 25, 2012; accepted June 8, 2012. Date of current version August 17, 2012. This work was supported by the National Science Foundation under Grant CCF-0811880. The review of this paper was arranged by Editor D. Esseni.

Y. Khatami, H. Li, and K. Banerjee are with the Department of Electrical and Computer Engineering, University of California at Santa Barbara, Santa Barbara, CA 93106 USA (e-mail: yasin@ece.ucsb.edu; hongli@ece.ucsb.edu; kaustav@ece.ucsb.edu).

C. Xu was with the Department of Electrical and Computer Engineering, University of California at Santa Barbara, Santa Barbara, CA 93106 USA. He is now with the Technology Development and Innovation Group, Maxim Integrated Products, Beaverton, OR 97005 USA (e-mail: Chuan.Xu@maxim-ic.com).

Color versions of one or more of the figures in this paper are available online at http://ieeexplore.ieee.org.

Digital Object Identifier 10.1109/TED.2012.2205257

0018-9383/$31.00 © 2012 IEEE

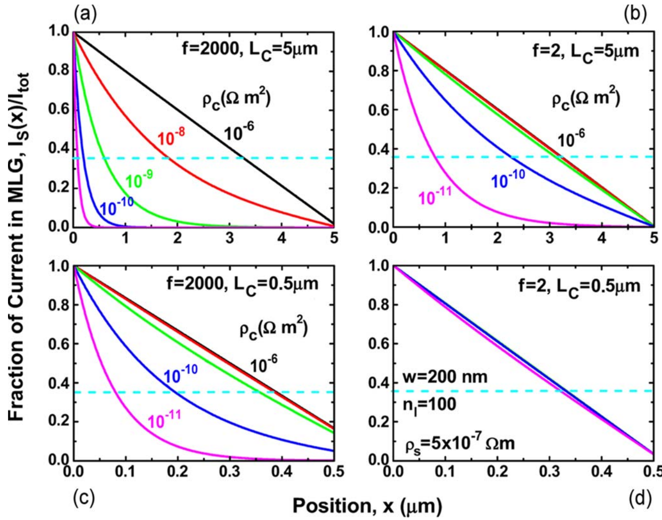

Fig. 1. Fraction of current in MLG as a function of position for different contact resistivities and with (a) $f = 2000$ and $L_C = 5\ \mu$m, (b) $f = 2$ and $L_C = 5\ \mu$m, (c) $f = 2000$ and $L_C = 0.5\ \mu$m, and (d) $f = 2$ and $L_C = 0.5\ \mu$m. ρ_c is varied between 10^{-11} and $10^{-6}\ \Omega \cdot \mathrm{m}^2$.

resistivity and the edge contact resistivity are represented by ρ_c and ρ_e, respectively, with units of ohm meter squared. The edge- and top-contact resistivities are related through $\rho_e = 2.92\rho_c/f$ [8], where f is the ratio of the top-contact resistivity per carbon atom to the edge-contact resistivity per carbon atom and varies between 0.01 and 10,000. The interlayer resistivity of MLG or the c-axis resistivity is represented by ρ_I with units of ohm meter [15]. In this paper, a wide range of resistivity values for metal, MLG, and contact is considered. This approach allows one to observe the contribution of the main resistances (namely, the metal resistivity, MLG sheet resistivity, and the contact resistivity) to the total resistance of the structure.

III. Model for Negligible Metal Resistance

The 1-D model with the assumption of negligible metal resistivity was developed in the companion paper [8]. In this section, the model is applied to metal-MLG contact structures. It is shown that the edge contacts can play an important role in the reduction of the total resistance of the metal-MLG structures. The assumption of negligible metal resistance is valid when the area of the metal is much larger than that of MLG. In this section, ρ_s is assumed to be larger than $5 \times 10^{-7}\ \Omega \cdot$ m, because lower values of ρ_s can lead to inaccurate results when ρ_m is ignored. The lower values of ρ_s are considered in Section IV, where a comprehensive model including the metal resistivity is developed. The top-contact resistivity is assumed to vary between 10^{-6} and $10^{-12}\ \Omega \cdot \mathrm{m}^2$ [9], [10], [16]–[34].

First, the current in MLG (I_S) along the contact length is normalized with respect to the total current of the structure [calculated from [8, eqs. (16) and (25)]], as shown in Fig. 1 for different parameters (n_l is the number of layers in MLG)

$$\frac{I_S(x)}{I_{\mathrm{tot}}} = \cosh(\beta x) - \frac{V}{A}\sinh(\beta x). \tag{1}$$

A and β are defined in [8]. The term $I_S(x)/I_{\mathrm{tot}}$ can be interpreted as the fraction of the total current passing through

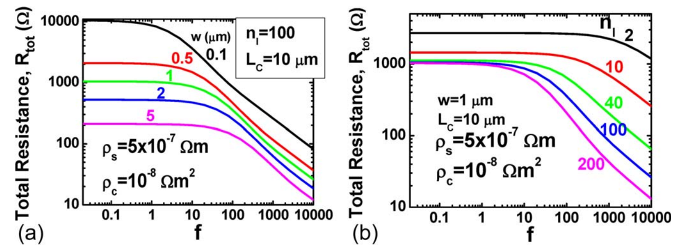

Fig. 2. Total resistance as a function of (a) f and w and (b) f and n_l.

the contact between x and L_C. This quantity can be used to determine the region over which the current crowding happens in a contact [14]. For example, the position x, where $I_S(x)/I_{\mathrm{tot}}$ becomes equal to $1/e$ [horizontal dashed line in Fig. 1], can be defined as the current crowding length (L_{cc}). By equating (1) to $1/e$ (or any desired value), the value of L_{cc} can be calculated. For the limit, where the contact length is much larger than L_{cc}, the contribution of side 3 to conduction becomes negligible and L_{cc} can be approximated by $1/\beta$.

In Fig. 1(a), the current distribution in MLG is plotted for a device with a large L_C (5 μm) and a large f for different values of contact resistivity. Due to the high value of f, the majority of current enters through the edge contacts, and L_{cc} is defined as the position x, where the curves cross the horizontal dashed line. As ρ_c (and, consequently, ρ_e) reduces, the overall contact resistance becomes smaller; therefore, the majority of the current passes through a small portion of the contact, and L_{cc} reduces. Fig. 1(b) shows the current distribution in MLG for the same parameters as in Fig. 1(a) but with a lower value of f. In this case, the overall contact resistance is higher than that of Fig. 1(a), and therefore, L_{cc} is larger. The importance of edge contacts can be observed by the comparison of Fig. 1(a) and (b), where a higher value of f leads to a significant reduction of L_{cc}. In Fig. 1(c), the current distribution is shown for a contact length of 0.5 μm and $f = 2000$. Due to the higher contribution of side 3 to conduction, the current is substantially higher at $x = L_C$ compared to Fig. 1(a). Subsequently, the dependence of L_{cc} on L_C becomes stronger, which can be deduced from [8, eq. (24)] and (1) through the parameter A. By the comparison of Fig. 1(c) and (d), it can be observed that, for low values of f, L_{cc} remains constant when ρ_c is varied. In this case, the contact resistance is the dominant resistance compared to the sheet/interlayer resistance, and the potential drop on the contact is large.

The total resistance of the contact–MLG structure (which includes both the contact resistance and MLG resistance) is another important factor that can be calculated from [8, eq. (25)]. The total resistance is simply the ratio of the total voltage on the contact to the total current

$$R_{\mathrm{tot}} = \frac{V}{-I_{\mathrm{tot}}} = \frac{\rho_s}{wt\beta}\frac{\frac{\rho_s}{\beta\rho_e}\tanh\beta L_C + 1}{\tanh\beta L_C + \frac{\rho_s}{\beta\rho_e}}. \tag{2}$$

In Fig. 2, the total resistance has been calculated as a function of width, thickness, and f. As can be seen by observing Fig. 2, the total resistance reduces by increasing the width or thickness (thickness is proportional to n_l). The total resistance is relatively independent of f for $f < 1$, where side 6 (top contact) contributes the most to R_{tot}, and the edge resistances are high.

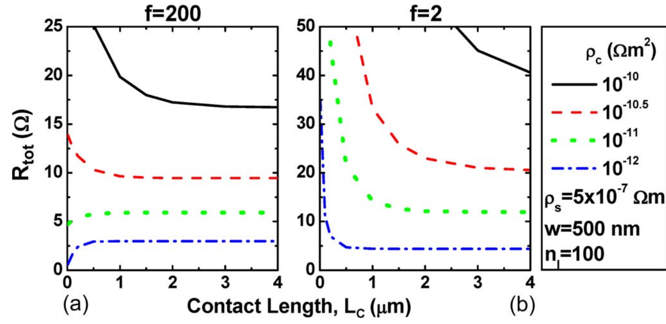

Fig. 3. Total resistance as a function of contact length and contact resistivity for (a) $f = 200$ and (b) $f = 2$.

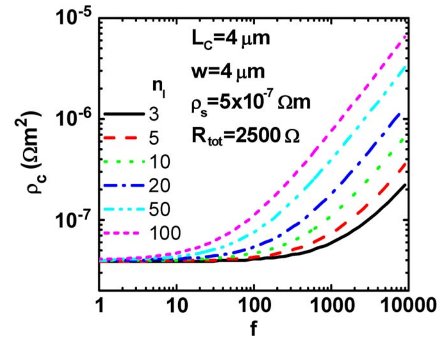

Fig. 4. Extracted contact resistivity from experiment and its dependence on f for various number of layers based on the developed model.

As f increases, the edge-contact resistivity becomes smaller, which leads to a smaller R_{tot}. It can be observed that good bonding between metal and edge carbons (which leads to a high f [9], [10]) is very effective in reducing the total resistance of the structure. For $f < 1$, the total resistance varies in a linear fashion with the inverse of w [Fig. 2(a)]. This trend is similar to conventional planar contact structures. For large values of f, the total resistance shows a linear relationship with the inverse of thickness [Fig. 2(b)]. In this regime, the side contacts 2 and 4 (see [8, Fig. 2]) contribute the most to conduction, and the total contact resistance of these two sides is inversely proportional to t.

Fig. 3 shows the total resistance as a function of contact length for different values of ρ_c and f. It can be observed from Fig. 3(a) that, for a high value of f, the total resistance approaches a constant value as L_C increases. In this regime, the current crowding length is much smaller than L_C, because of the low contact resistivity. An interesting trend can be observed when L_C is reduced. For high values of ρ_c, the total resistance increases as L_C reduces, while for low values of ρ_c, the total resistance decreases as L_C reduces. In the former regime, the contact resistance is the dominant resistance. The reason is that the sheet resistance reduces as L_C becomes smaller, while contact resistance increases due to lower contact area. Subsequently, the sheet resistance of MLG is dominant for low values of ρ_c. The total resistance shows a different trend in Fig. 3(b), where R_{tot} increases as L_C becomes smaller than L_{cc}. In this case, due to the smaller value of f, the contact resistivity is always higher than that of Fig. 3(a), and the contact resistivity is the major component of R_{tot}.

For large values of L_C, the total resistance can be approximated by $\rho_s/wt\beta$, which can be simplified to $(\rho_k\rho_s/wt)^{1/2}$. In the limit where L_C approaches zero, the total resistance becomes equal to the total resistance of side 3, ρ_e/wt. The results indicate that, in the absence of edge contacts, the contact resistance is the main contributor to the total resistance of the metal-MLG structures. Even for values of ρ_c down to 10^{-12} $\Omega \cdot \text{m}^2$ (low f), the contact resistance is the dominant resistance in the system. However, the incorporation of the edge contacts can greatly reduce the total resistance of the structure. It should be noted that the reduction of the total resistance by the use of edge contacts also depends on the width and thickness of the structure as shown in Fig. 2.

To further illustrate the effect of edge contacts on the characterization of the metal-MLG structure, the extracted contact resistivity is shown in Fig. 4 as a function of f for various number of layers when R_{tot} is constant. A typical device with the width and contact length of 4 μm is considered. The total resistance is assumed to be 2500 Ω, which is a typical value reported in [12] for various number of layers. It can be observed from Fig. 4 that, for low values of f (where edge contact is negligible), the extracted contact resistivity approaches a constant value, which is independent of the number of layers. In this regime, the analysis based only on the top-contact model [9]–[12], [16]–[34] is valid. However, as f increases, ρ_c increases, and its value becomes a strong function of f. This analysis shows that the value of ρ_c is underestimated if the edge contacts are neglected. Moreover, lower values of R_{tot} are also reported in the literature [11], [12]. The dependence of the extracted ρ_c on the number of layers becomes stronger as the total resistance reduces, because the effect of MLG sheet resistivity becomes more important.

IV. Model and Analysis Including Metal Resistance

In this section, a 1-D model is developed for the device structure shown in [8, Fig. 2] by considering the metal resistivity. The effect of metal resistance on the total resistance of the metal-MLG structure will be discussed. The 1-D model is compared to the 3-D numerical simulation of the system to derive a valid model. The 3-D system is only solved numerically in this case, because of the complexity of the 3-D PDE system. The metal resistivity is varied between 2×10^{-8} and 3×10^{-7} $\Omega \cdot \text{m}$. In conventional silicon-based transistors, ρ_m is typically very small compared to the sheet resistivity of silicon and can be ignored, but in the case of graphene, due to its small sheet resistivity, the metal resistivity plays an important role in determining the contact resistance and the distribution of current over the contact area. Typically, the metal resistivity becomes more important when ρ_m and ρ_s become comparable.

A. Model Derivation

The 1-D schematic model of the system is adopted from [8, Fig. 4]. It is assumed that the potential variation along the x-axis is negligible at $x > L_C + L_m$ (for example, because of the metal pad or wider metal interconnect). Therefore, the metal is connected to a voltage source V_{DD} at $x = L_C + L_m$. The extension of the metal between $x = L_C$ and $x = L_C + L_m$ is modeled with the resistance $\rho_m L_m/w_t t_t$, which is in series

with the total resistance of the structure R_{tot} (from $x = 0$ to $x = L_C$), and w_t and t_t are the total width and thickness of the metal, respectively. Therefore, in this section, only the portion of the metal between $x = 0$ and $x = L_C$ is considered, and all the potentials are calculated with respect to the potential in the metal, $V_m = V$, at $x = L_C$.

From the structure shown in [8], by defining the area of the metal surrounding MLG, S_m, and the ratio of metal area to MLG area s_r as

$$S_m = w_t t_t - wt \tag{3}$$

$$s_r = \frac{wt}{S_m} \tag{4}$$

the current distribution in the metal can be written as

$$I_m(x) = \frac{-wt}{s_r \rho_m} \frac{dV_m}{dx}. \tag{5}$$

The current distribution in MLG is defined by [8, eq. (16)]. The system of PDEs for the structure can be written as

$$\frac{d^2 V_S}{dx^2} - \frac{\rho_s}{wt\rho_k}(V_S - V_m) = 0 \tag{6}$$

$$\frac{d^2 V_m}{dx^2} + \frac{s_r \rho_m}{wt\rho_k}(V_S - V_m) = 0 \tag{7}$$

which has a general solution of the form

$$V_S(x) = \frac{\rho_s}{\rho_s + s_r\rho_m}[A \sinh \beta x + B \cosh \beta x] + Dx + C \tag{8}$$

$$V_m(x) = \frac{-s_r\rho_m}{\rho_s + s_r\rho_m}[A \sinh \beta x + B \cosh \beta x] + Dx + C \tag{9}$$

$$\beta = \sqrt{\frac{\rho_s + s_r\rho_m}{wt\rho_k}}. \tag{10}$$

The boundary conditions for this system are

$$\text{at } x = 0 : V_S(0) = 0 \tag{11}$$

$$\text{at } x = 0 : \frac{dV_m}{dx} = 0 \tag{12}$$

$$\text{at } x = L_C : V_m(L_C) = V \tag{13}$$

$$\text{at } x = L_C : I_S = \frac{wt}{\rho_e}(V_S - V). \tag{14}$$

By applying the B.C. to the system, all the constants A, B, C, and D can be calculated in (15)–(18), shown at the bottom of the page, where

$$F_1 = \frac{\rho_s \cosh \beta L_C + \beta\rho_e \sinh \beta L_C - \rho_s}{s_r\rho_m \cosh \beta L_C + \rho_s} \tag{19}$$

$$F_2 = \beta\rho_e \cosh \beta L_C + \rho_s \sinh \beta L_C + s_r\rho_m\beta\left(L_C + \frac{\rho_e}{\rho_s}\right). \tag{20}$$

The total current is equal to $I_S(x = 0)$ and is calculated from [8, eq. (25)]. The total resistance including the metal, contact, and MLG resistances is given by (21)–(23), shown at the bottom of the page, where R_L represents the geometrical line resistance and R_C is the contact resistance. The contribution of sides 2, 4, and 6 ([8, Fig. 2]) is reflected in (21)–(23) through β which depends on ρ_k, and the contribution of side 3 is reflected through ρ_e.

Next, the contact resistivity ρ_k is adjusted to fit the 1-D and 3-D models. By a similar approach as in the companion paper [8] (a first-order approximation), the effective contact resistivities ρ_c^* and ρ_e^* are defined

$$\rho_c^* = \rho_c + \alpha_{\text{cs}} t\rho_I + \alpha_{\text{cm}} t_{\text{sm}} \rho_m \frac{wt_{\text{sm}}}{S_m} \tag{24}$$

$$\rho_e^* = \rho_e + \alpha_{\text{es}} w\rho_s + \alpha_{\text{em}} w_{\text{sm}} \rho_m \frac{2w_{\text{sm}} t}{S_m} \tag{25}$$

$$C = \frac{-\rho_s}{\rho_s + s_r\rho_m} B \tag{15}$$

$$D = \frac{s_r\rho_m\beta}{\rho_s + s_r\rho_m} A \tag{16}$$

$$A = \frac{(\rho_s + s_r\rho_m)(1 + F_1)}{F_2 + s_r\rho_m F_1(\beta L_C - \sinh \beta L_C)} V \tag{17}$$

$$B = \frac{(\rho_s + s_r\rho_m)\left[s_r\rho_m(\beta L_C - \sinh \beta L_C) - F_2\right]}{\left[F_2 + s_r\rho_m F_1(\beta L_C - \sinh \beta L_C)\right]\left[s_r\rho_m \cosh \beta L_C + \rho_s\right]} V \tag{18}$$

$$R_{\text{tot}} = \frac{V}{-I_{\text{tot}}} = R_L + R_C \tag{21}$$

$$R_L = \frac{s_r\rho_m\rho_s}{(\rho_s + s_r\rho_m)} \frac{L_C}{wt} \tag{22}$$

$$R_C = \frac{\beta\rho_e\left[\left(\rho_s^2 + s_r^2\rho_m^2\right)\cosh \beta L_C + 2\rho_s s_r\rho_m\right] + \rho_s^2(\rho_s + s_r\rho_m)\sinh \beta L_C}{wt\beta(\rho_s + s_r\rho_m)\left[(\rho_s + s_r\rho_m)\cosh \beta L_C + \beta\rho_e \sinh \beta L_C\right]} \tag{23}$$

where $\alpha_{\rm cs}$ and $\alpha_{\rm es}$ account for the nonzero thickness and width of the MLG, respectively, and $\alpha_{\rm cm}$ and $\alpha_{\rm em}$ account for the nonzero thickness and width of the metal, respectively. The third term on the right-hand side of (25) has an extra term $2w_{\rm sm}t/S_m$. This extra term scales the metal resistivity in the y-direction (in 3-D system) with the metal thickness. A thicker metal has a smaller resistance in the y-direction, which leads to a smaller 3-D potential variation along the y-axis in the metal. In addition, the portion of metal covering the top side of MLG further reduces the total resistance of the metal, and the overall effect is reflected in S_m. A similar argument for $\alpha_{\rm cm}$ leads to (24).

The distribution of current in the metal in the 3-D system along the y- and z-directions was also investigated for possible current crowding effects along these directions (where only an effective area of metal contributes to conduction). The current density along the x-axis is high near the metal-MLG interface and reduces toward the outer edge of the metal. However, the current density near the outer edge is comparable to the current density at the metal-MLG interface, and a current crowding effect was not observed for the considered dimensions of $w_{\rm sm}$ and $t_{\rm sm}$ up to 2 μm.

The optimized value of the remaining coefficients in (24) and (25) is calculated by comparing the 1-D and 3-D simulation results similar to the method described in [8, Sec. III-B]. The optimized values are $\alpha_{\rm cs} = 0.25$, $\alpha_{\rm es} = 0.12$, $\alpha_{\rm cm} = 0.3$, and $\alpha_{\rm em} = 0.21$. A trend similar to the one in the 1-D model with a negligible metal resistivity was observed for the range of validity of the model. For $\rho_e/w\rho_s$, $\rho_c/t\rho_I$, $\rho_e S_m/2w_{\rm sm}^2 t\rho_m$, and $\rho_c S_m/wt_{\rm sm}^2\rho_m$ values larger than 1.0, accurate fitting is achieved between the 1-D and 3-D models.

B. Results and Discussion

The metal resistance becomes important as the MLG sheet resistance and the contact resistance become smaller. The 1-D model is used to determine the conditions for which the metal resistance needs to be considered. It can be observed from the equivalent 1-D circuit model [8, Fig. 4] that the contact structure is almost symmetric (except for the contribution of the term ρ_e/wt) with respect to the sheet resistances of metal and MLG between $x = 0$ and $x = L_C$. Therefore, the relative magnitude of the resistances $\rho_m dx/S_m$ and $\rho_s dx/wt$ (refer to [8, Fig. 4]) can be used to determine the dominant resistance in the structure. Since dx is the same for both resistances, only the resistance per length values, ρ_m/S_m and ρ_s/wt, are considered. Alternatively, $s_r\rho_m$ and ρ_s can be used [refer to (4)] for comparison of the relative resistances of metal and MLG sheets.

Fig. 5 shows the total resistance of the contact structure, for different resistance per length values of metal and MLG and different values of contact resistivity. The reported data are shown for $w_{\rm sm} = 50$ nm to 1 μm, $\rho_m = 2\times10^{-8}$ to 3×10^{-7} $\Omega\cdot$m, $w = 500$ nm, and $\rho_s = 5\times10^{-8}$ to 5×10^{-9} $\Omega\cdot$m. It can be observed from Fig. 5(c) that $R_{\rm tot}$ is a weak function of ρ_m/S_m for $\rho_c = 10^{-9}$ $\Omega\cdot$m^2 and $f = 200$. In this regime, the contact resistance and the MLG sheet resistance are the dominant resistances of the structure. As ρ_c and ρ_s/wt become

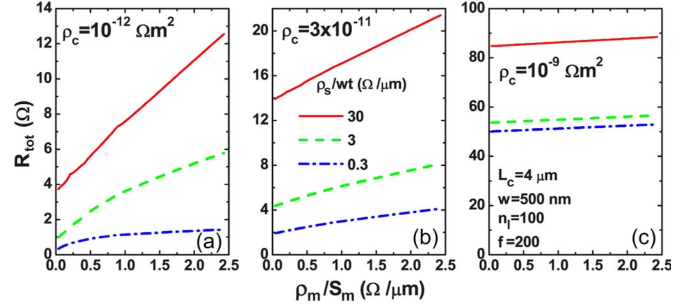

Fig. 5. Total resistance as a function of metal and MLG resistances per unit length for three values of ρ_c. The contribution of metal resistance becomes more prominent for low values of ρ_c.

smaller, the contribution of the metal sheet resistivity becomes more observable as shown in Fig. 5(a) and (b).

The total resistance shows a strong dependence on ρ_m/S_m as shown in Fig. 5(b). As contact resistivity further reduces [Fig. 5(a)], the contribution of metal resistance becomes more important. In this case, the sheet resistivities of MLG and metal are the dominant resistances in the system. As expected, an increase of the ρ_m/S_m value leads to a higher $R_{\rm tot}$, and it can be observed that the variation of ρ_m/S_m can lead to a variation of the total resistance several times the original value.

Copper and gold have resistivity values around 2×10^{-8} $\Omega\cdot$m, and their resistivity further increases as the dimensions scale down. For a value of $\rho_m = 2\times10^{-8}$ $\Omega\cdot$m and a total metal width and thickness of 500 nm, ρ_m/S_m is around 8×10^4 Ω/m, which falls into the range shown in Fig. 5(a). Although the experimental contact resistivity values reported for metal–graphene structures are usually high [11], [12], [16]–[23], the theoretical studies show that the contact resistivity can potentially become very small particularly for MLG considering the edge contacts [9], [10], [35]–[37]. Therefore, in the edge-contacted structures, it is important to understand and consider the role of metal resistance, since a neglecting of its effects can lead to errors in measurement of the contact resistivity. The measured contact resistivity would be higher than its real value if the metal resistance is ignored. The effect of the metal resistivity becomes more prominent when the extension of metal from $x = L_C$ to $x = L_C + L_M$ is taken into account.

Fig. 6 shows the contact current per unit length (I_{C1D})

$$I_{C1D} = \frac{V_m - V_S}{\rho_k} \tag{26}$$

and the portion of current in MLG along the length of the structure for different values of resistance per unit length in MLG ($IC1D$ is the current flowing through the contact resistances ρ_k/dx). The effect of the sheet resistivity on the current distribution can be observed from this figure. ρ_m/S_m has a constant value, but ρ_s/wt varies between values lower and higher than ρ_m/S_m. A relatively small value of contact resistivity is chosen, so that the effect of sheet resistance becomes more obvious. Similar to the approach in Section III, the current crowding length can be calculated by equating the fraction of current in MLG $(I_S(x)/I_{\rm tot})$ to a predefined value.

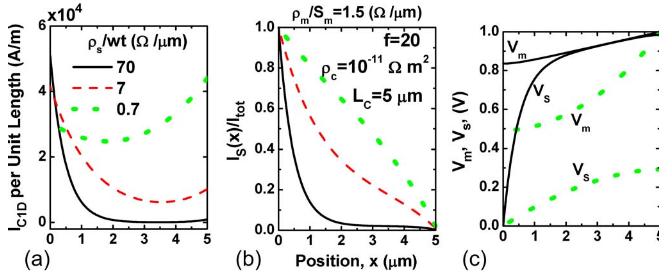

Fig. 6. Current and voltage distribution along the contact length in the metal-MLG contact structure for different values of MLG resistance per unit length. (a) Contact current per unit length. (b) Fraction of current in MLG. (c) Voltage distribution along the length in metal and MLG. $w = 200$ nm, $n_l = 100$, $w_{\mathrm{sm}} = 200$ nm, and $t_{\mathrm{sm}} = 200$ nm.

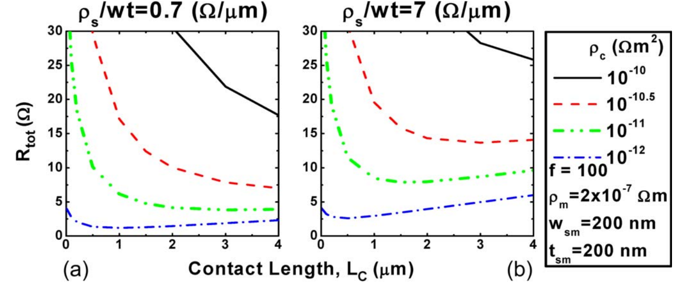

Fig. 7. Total resistance as a function of contact length and contact resistivity for different values of MLG resistance per unit length. $w = 400$ nm and $n_l = 50$.

It can be seen by observing Fig. 6(a) and (b) that the metal-MLG structure exhibits a behavior similar to conventional structures for high values of $\rho_s/wt = 7 \times 10^7\ \Omega/\mathrm{m}$, where current crowding can be seen by observing the fraction of current in MLG. As ρ_s/wt reduces, the metal resistance contributes more to the total resistance, and the current distribution in contact and MLG changes. For $\rho_s/wt = 7 \times 10^5\ \Omega/\mathrm{m}$, about 50% of the current enters the MLG within $x = 2.5$ and 5 μm [Fig. 6(b)]. In this case, L_{cc} is larger than the contact length, because the current passes through the entire contact structure. The origin of the current distribution in Fig. 6(a) and (b) can be understood from Fig. 6(c) [and referring to (26)], where the potential distribution in metal and in MLG is shown for $\rho_s/wt = 7 \times 10^5\ \Omega/\mathrm{m}$ and $\rho_s/wt = 7 \times 10^7\ \Omega/\mathrm{m}$. For a high value of ρ_s/wt, the total potential drop in MLG is high, and therefore, most of the current passes through the end of the contact ($x = 0$). On the other hand, for a lower value of ρ_s/wt, all the three major components of resistance (metal, MLG, and contact) show a somewhat equal potential drop. Subsequently, the current passes through the entire area of the contact. An interesting fact about this structure is that the amount of current entering through the right half of the contact can become higher than that of the left half, which should be taken into account in optimizing the contact area.

In Fig. 7, the total resistance of the structure has been calculated using (21) as a function of L_C for various values of ρ_c. For $\rho_c = 10^{-10}\ \Omega \cdot \mathrm{m}^2$, R_{tot} increases as L_C becomes small, due to the dominance of the contact resistance. Larger values of ρ_c lead to a behavior similar to the case where $\rho_c = 10^{-10}\ \Omega \cdot \mathrm{m}^2$ and are not shown in the figure. As ρ_c becomes smaller, the sheet resistivity becomes important. From Fig. 7, for low values of ρ_c, the total resistance reduces with a reduction in L_C. The reduction of R_{tot} indicates that the geometrical line resistance (R_L) is the dominant resistance in this regime, because, generally, a reduction in L_C leads to a higher contact resistance and a lower sheet resistance. As L_C further reduces, the total resistance exhibits a different behavior, and it increases abruptly. In this regime, the contact resistance (R_C) becomes dominant.

The total resistance increases abruptly as the contact length becomes smaller than the current crowding length. The value of L_{cc} can be approximated by $1/\beta$. Although the effect of side 3 is neglected by this approximation, it still provides a relatively accurate estimation for contact resistivity values studied in this work. As L_C goes to infinity, the total resistance becomes infinite [refer to (22)], which is different than the behavior observed when ignoring the metal resistivity. In the limit where L_C becomes zero, the total resistance approaches ρ_e/wt.

V. Contact Resistance in the Quasi-Ballistic Regime

The presented results were provided under the assumption of negligible quantum resistance, which is valid in the diffusive regime. The quantum resistance can become dominant in graphene structures in the quasi-ballistic to ballistic regime. The generalization of the presented model to quasi-ballistic regime is provided in this section.

The contact resistance for a nanowire in the quasi-ballistic regime is discussed in [38]. Similarly, the current and voltage in graphene are described by $dI_S/dx = -2\chi(V - V_S)/R_{Q,W}$ and $dV_S/dx = -R_{Q,W}(\phi + \chi/2)I_S$. These equations can be compared to [8, eqs. (16) and (17)]. $R_{Q,W}$ is the ballistic resistance for graphene with width w, ϕ is the scattering probability per unit length, and χ is defined as $R_{Q,W}/2\rho_k$. The purely ballistic and diffusive regimes are associated with $\phi \rightarrow 0$ and $\phi \rightarrow \infty$, respectively. For a hypothetical narrow graphene layer with one mode contributing to transport, $R_{Q,W} = h/2q^2$, where h is Planck's constant and q is the unit electronic charge.

In this context, the sheet resistivity of graphene under the contact is $\rho_{S,C} = wtR_{Q,W}(\phi + \chi/2)$, which means that $\rho_{S,C}$ depends on the contact resistivity. It is worth mentioning that $\rho_{S,C}$ has a nonzero value even in the ballistic regime. The sheet resistivity of a graphene sheet with no contact is $\rho_s = wtR_{Q,W}\phi$, therefore

$$\rho_{S,C} = \rho_s + \frac{wt}{4\rho_k} R_{Q,W}^2. \tag{27}$$

In the quasi-ballistic regime, the sheet resistivity (ρ_s) of the developed model in earlier sections should be replaced by (27) to include the effect of quantum resistance. It can be shown that $R_{Q,W}$ is proportional to w^{-1} [39]. According to [8, eq. (30)], ρ_k is also proportional to w^{-1} for the top-contact structure, which means that $\rho_{S,C}$ is independent of w for a top-contact structure. According to (27), a higher value of sheet resistivity for graphene under contact should be incorporated (compared to the sheet resistivity of the channel) to account for the quantum resistance.

The higher sheet resistivity under the contact is a barrier in reducing the total resistance of the contact particularly when the contact resistivity is low. This limitation can be compensated for by increasing the carrier density (which is tightly related to the Fermi level) of graphene layers or by increasing the number of layers. As stated in the companion paper [8], the metal electrodes can alter the Fermi level in graphene layers which would be advantageous and worth in-depth investigation. Intercalation doping of graphene is another effective method for charge injection [40].

VI. Conclusion

The characteristics of the contact between metal electrode and MLG have been studied by developing a rigorous 1-D model that includes both edge and top contacts for the first time. The 1-D model has been designed to include the effects of potential variation along the width and thickness of the structure. The major sources of contact resistance—MLG sheet resistivity, metal sheet resistivity, and contact resistivity—have been included in the model. The 1-D model is valid under the following assumptions: 1) ohmic contact between metal and MLG; 2) negligible edge scattering; 3) contact width less than twice the contact length; 4) low voltage bias (0.1 V); and 5) values of $\rho_e/w\rho_s$, $\rho_c/t\rho_I$, $\rho_e S_m/2w_{\rm sm}^2 t\rho_m$, and $\rho_c S_m/wt_{\rm sm}^2\rho_m$ larger than one. The 1-D model has been applied to the metal-MLG structure for the analysis of the characteristics of the system. The results have been obtained by varying the geometry of the contact and the resistivity values as follows: 1) $10^{-12} < \rho_c < 10^{-6}\ \Omega\cdot{\rm m}^2$; 2) $2\times10^{-8} < \rho_m < 3\times10^{-7}\ \Omega\cdot{\rm m}$; 3) $5\times10^{-9} < \rho_s < 5\times10^{-7}\ \Omega\cdot{\rm m}$; and 4) $0.01 < f < 10000$.

The current crowding effects have been investigated. It has been shown that, because of the low sheet resistivity of MLG, the metal resistance can become the major component of the total resistance particularly as the dimensions scale down. It has been shown that the parameters ρ_s/wt and ρ_m/S_m can be used to determine the relative importance of metal and MLG sheet resistivity values. It can be observed that, for $\rho_s/wt \gg \rho_m/S_m$, the metal resistivity can be ignored. However, this is a rough estimate, and only a careful examination of the potential drop on metal, contact, and MLG (using the 1-D model) can produce accurate results.

It has been shown that the edge contacts greatly reduce the total resistance of the metal–MLG structure. The level of improvement depends on the geometry and sheet resistivity of MLG and metal. The higher the number of layers of MLG, the higher is the contribution of the edge contacts to conduction. Thus, for metals that have a strong edge bonding with graphene, a higher number of layers provides an advantage. A higher contact width reduces the total resistance of the structure and increases the contribution of the top contact to conduction. A smaller contact length reduces the sheet resistance which leads to lower total resistance, but a small contact length can lead to extreme current crowding in the system that increases the total resistance. For contact structures with a low edge-contact resistivity, the current crowding length can be reduced significantly.

The contact resistance has been also discussed in the quasi-ballistic transport regime. It is shown that the effective sheet resistivity of graphene under the contact can be modified to account for quantum resistance. In summary, the analysis in this work provides a better understanding of the contact in metal–MLG structures and can provide invaluable insight into the characterization and efficient design of contact structures.

Acknowledgment

The authors would like to thank the Center for Scientific Computing at the CNSI and MRL, an NSF MRSEC (DMR-1121053) and NSF CNS-0960316, for the computing support.

References

[1] J.-H. Chen, C. Jang, S. Xiao, M. Ishigami, and M. S. Fuhrer, "Intrinsic and extrinsic performance limits of graphene devices on SiO_2," *Nature Nanotechnol.*, vol. 3, no. 4, pp. 206–209, Apr. 2008.

[2] S. V. Morozov, K. S. Novoselov, M. I. Katsnelson, F. Schedin, D. C. Elias, J. A. Jaszczak, and A. K. Geim, "Giant intrinsic carrier mobilities in graphene and its bilayer," *Phys. Rev. Lett.*, vol. 100, no. 1, pp. 016602-1–016602-4, Jan. 2008.

[3] Y. Awano, "Graphene for VLSI: FET and interconnect applications," in *Proc. IEDM*, 2009, pp. 1–4.

[4] X. Chen, D. Akinwande, K.-J. Lee, G. F. Close, S. Yasuda, B. C. Paul, S. Fujita, J. Kong, and H. P. Wong, "Fully integrated graphene and carbon nanotube interconnects for gigahertz high-speed CMOS electronics," *IEEE Trans. Electron Devices*, vol. 57, no. 11, pp. 3137–3143, Nov. 2010.

[5] A. N. Pal and A. Ghosh, "Ultralow noise field-effect transistor from multilayer graphene," *Appl. Phys. Lett.*, vol. 95, no. 8, pp. 082105-1–082105-3, Aug. 2009.

[6] C.-J. Shih, A. Vijayaraghavan, R. Krishnan, R. Sharma, J.-H. Han, M.-H. Ham, Z. Jin, S. Lin, G. L. C. Paulus, N. F. Reuel, Q. H. Wang, D. Blankschtein, and M. S. Strano, "Bi- and trilayer graphene solutions," *Nature Nanotechnol.*, vol. 6, no. 7, pp. 439–445, Jul. 2011.

[7] A. A. Balandin, "Thermal properties of graphene, carbon nanotubes and nanostructured carbon materials," *Nature Mater.*, vol. 10, no. 8, pp. 569–581, 2011.

[8] Y. Khatami, H. Li, C. Xu, and K. Banerjee, "Metal-to-multilayer-graphene contact—Part I: Contact resistance modeling," *IEEE Trans. Electron Devices*, vol. 59, no. 9, pp. 2444–2452, Sep. 2012.

[9] Y. Matsuda, W.-Q. Deng, and W. A. Goddard, "Contact resistance for 'end-contacted' metal–graphene and metal–nanotube interfaces from quantum mechanics," *J. Phys. Chem. C*, vol. 114, no. 41, pp. 17 845–17 850, 2010.

[10] C. Gong, G. Lee, W. Wang, B. Shan, E. M. Vogel, R. M. Wallace, and K. Cho, "First-principles and quantum transport studies of metal–graphene end contacts," in *Proc. MRS*, 2010, pp. 1259-S14–1259-S35.

[11] A. Venugopal, L. Colombo, and E. M. Vogel, "Contact resistance in few and multilayer graphene devices," *Appl. Phys. Lett.*, vol. 96, no. 1, pp. 013512-1–013512-3, Jan. 2010.

[12] K. Nagashio, T. Nishimura, K. Kita, and A. Toriumi, "Systematic investigation of the intrinsic channel properties and contact resistance of monolayer and multilayer graphene field-effect transistor," *Jpn. J. Appl. Phys.*, vol. 49, no. 5, p. 051304, 2010.

[13] H. Berger, "Models for contacts to planar devices," *Solid State Electron.*, vol. 15, no. 2, pp. 145–158, Feb. 1972.

[14] D. B. Scott, W. R. Hunter, and H. Shichijo, "A transmission line model for silicided diffusions: Impact on the performance of VLSI circuits," *IEEE Trans. Electron Devices*, vol. ED-29, no. 4, pp. 651–661, Apr. 1982.

[15] D. Z. Tsang and M. S. Dresselhaus, "The c-axis electrical conductivity of kish graphite," *Carbon*, vol. 14, no. 1, pp. 43–46, 1976.

[16] J. H. LeeEduardo, K. Balasubramanian, R. T. Weitz, M. Burghard, and K. Kern, "Contact and edge effects in graphene devices," *Nature Nano*, vol. 3, no. 8, pp. 486–490, 2008.

[17] K. Nagashio, T. Nishimura, K. Kita, and A. Toriumi, "Contact resistivity and current flow path at metal/graphene contact," *Appl. Phys. Lett.*, vol. 97, no. 14, pp. 143 514-1–143 514-3, Oct. 2010.

[18] J. A. Robinson, M. LaBella, M. Zhu, M. Hollander, R. Kasarda, Z. Hughes, K. Trumbull, R. Cavalero, and D. Snyder, "Contacting

graphene," *Appl. Phys. Lett.*, vol. 98, no. 5, pp. 053103-1–053103-3, Jan. 2011.

[19] F. Xia, V. Perebeinos, Y.-M. Lin, Y. Wu, and P. Avouris, "The origins and limits of metal–graphene junction resistance," *Nature Nanotechnol.*, vol. 6, no. 3, pp. 179–184, Feb. 2011.

[20] K. L. Grosse, M.-H. Bae, F. Lian, E. Pop, and W. P. King, "Nanoscale Joule heating, Peltier cooling and current crowding at graphene–metal contacts," *Nature Nanotechnol.*, vol. 6, no. 5, pp. 287–290, May 2011.

[21] B. C. Huang, M. Zhang, Y. Wang, and J. Woo, "Contact resistance in top-gated graphene field-effect transistors," *Appl. Phys. Lett.*, vol. 99, no. 3, pp. 032107-1–032107-3, Jul. 2011.

[22] V. K. Nagareddy, I. P. Nikitina, D. K. Gaskill, J. L. Tedesco, C. R. Eddy, J. P. Goss, N. G. Wright, and A. B. Horsfall, "High temperature measurements of metal contacts on epitaxial graphene," *Appl. Phys. Lett.*, vol. 99, no. 7, pp. 073506-1–073506-3, Aug. 2011.

[23] M. Nagase, H. Hibino, H. Kageshima, and H. Yamaguchi, "Contact conductance measurement of locally suspended graphene on SiC," *Appl. Phys. Exp.*, vol. 3, no. 4, pp. 045101-1–045101-3, 2010.

[24] R. Nouchi, T. Saito, and K. Tanigaki, "Determination of carrier type doped from metal contacts to graphene by channel-length-dependent shift of charge neutrality points," *Appl. Phys. Exp.*, vol. 4, no. 3, pp. 031501-1–031501-12, Mar. 2011.

[25] N. Park, B.-K. Kim, J.-O. Lee, and J.-J. Kim, "Influence of metal work function on the position of the Dirac point of graphene field-effect transistors," *Appl. Phys. Lett.*, vol. 95, no. 24, pp. 243 105-1–243 105-3, Dec. 2009.

[26] K. N. Parrish and D. Akinwande, "Impact of contact resistance on the transconductance and linearity of graphene transistors," *Appl. Phys. Lett.*, vol. 98, no. 18, pp. 183 505-1–183 505-3, May 2011.

[27] N. Xu and J. W. Ding, "Conductance growth in metallic bilayer graphene nanoribbons with disorder and contact scattering," *J. Phys., Condens. Matter*, vol. 20, no. 48, p. 485 213, Dec. 2008.

[28] Y.-B. Zhou, B.-H. Han, Z.-M. Liao, Q. Zhao, J. Xu, and D.-P. Yu, "Effect of contact barrier on electron transport in graphene," *J. Chem. Phys.*, vol. 132, no. 2, pp. 024706-1–024706-5, Jan. 2010.

[29] S. Barraza-Lopez, M. Vanević, M. Kindermann, and M. Y. Chou, "Effects of metallic contacts on electron transport through graphene," *Phys. Rev. Lett.*, vol. 104, no. 7, pp. 076807-1–076807-4, Feb. 2010.

[30] D. Berdebes, T. Low, Y. Sui, J. Appenzeller, and M. S. Lundstrom, "Substrate gating of contact resistance in graphene transistors," *IEEE Trans. Electron Devices*, vol. 58, no. 11, pp. 3925–3932, Nov. 2011.

[31] P. Blake, R. Yang, S. V. Morozov, F. Schedin, L. A. Ponomarenko, A. A. Zhukov, I. V. Grigorieva, K. S. Novoselov, and A. K. Geim, "Influence of metal contacts and charge inhomogeneity on transport properties of graphene near the neutrality point," *Solid State Commun.*, vol. 149, no. 27, pp. 1068–1071, Jul. 2009.

[32] J. Cayssol, B. Huard, and D. Goldhaber-Gordon, "Contact resistance and shot noise in graphene transistors," *Phys. Rev. B*, vol. 79, no. 7, pp. 0754280-1–0754280-6, Feb. 2008.

[33] A. Hsu, H. Wang, K. K. Kim, J. Kong, and T. Palacios, "Impact of graphene interface quality on contact resistance and RF device performance," *IEEE Electron Device Lett.*, vol. 32, no. 8, pp. 1008–1010, Aug. 2011.

[34] T. Mueller, F. Xia, M. Freitag, J. Tsang, and P. Avouris, "The role of contacts in graphene transistors: A scanning photocurrent study," *Phys. Rev. B*, vol. 79, no. 24, pp. 245 430-1–245 430-6, Jun. 2009.

[35] P. A. Khomyakov, G. Giovannetti, P. C. Rusu, G. Brocks, J. van den Brink, and P. J. Kelly, "First-principles study of the interaction and charge transfer between graphene and metals," *Phys. Rev. B*, vol. 79, no. 19, pp. 195 425-1–195 425-12, May 2009.

[36] C. Gong, G. Lee, B. Shan, E. M. Vogel, R. M. Wallace, and K. Cho, "First-principles study of metal–graphene interfaces," *J. Appl. Phys.*, vol. 108, no. 12, pp. 123 711-1–123 711-8, Dec. 2010.

[37] Q. Ran, M. Gao, X. Guan, Y. Wang, and Z. Yu, "First-principles investigation on bonding formation and electronic structure of metal–graphene contacts," *Appl. Phys. Lett.*, vol. 94, no. 10, pp. 103 511-1–103 511-3, Mar. 2009.

[38] P. M. Solomon, "Contact resistance to a one-dimensional quasi-ballistic nanotube/wire," *IEEE Electron Device Lett.*, vol. 32, no. 3, pp. 246–248, Mar. 2011.

[39] S. Datta, *Electronic Transport in Mesoscopic Systems*. Cambridge, U.K.: Cambridge Univ. Press, 1995.

[40] M. S. Dresselhaus and G. Dresselhaus, "Intercalation compounds of graphite," *Adv. Phys.*, vol. 33, no. 51, p. 228, Dec. 2002.

Yasin Khatami (S'05) received the B.Sc. and M.Sc. degrees in EE from Sharif University of Technology, Tehran, Iran. He is currently working toward the Ph.D. degree at the University of California, Santa Barbara, in the field of graphene electronics and energy-efficient devices.

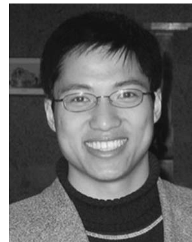

Hong Li (S'07) received the M.S. degree from Shanghai Jiao Tong University, Shanghai, China. He is currently working toward the Ph.D. degree in the Department of Electrical and Computer Engineering, University of California, Santa Barbara.

Chuan Xu (S'08–M'12) received the B.S. and the M.S. degrees in microelectronics from Peking University in 2004 and 2007, respectively, and the Ph.D. degree in electrical engineering from University of California, Santa Barbara.

Dr. Xu is now with Maxim Integrated Products, Beaverton, Oregon.

Kaustav Banerjee (S'92–M'99–SM'03–F'12) received the Ph.D. degree in electrical engineering and computer sciences from the University of California, Berkeley, in 1999.

He is currently a Professor in the Department of Electrical and Computer Engineering at the University of California, Santa Barbara, working on nanoelectronics.